



Original Articles

Neovascularization directed by CAVIN1/CCBE1/VEGFC confers TMZ-resistance in glioblastoma



Mei Wang ^{a,b,1}, Die Xia ^{a,b,1}, Daxing Xu ^{a,b}, Ying Yin ^{a,b}, Fei Xu ^c, Bo Zhang ^{a,b}, Koukou Li ^{a,b}, Zhenkun Yang ^{a,b}, Jian Zou ^{a,b,*}

^a Department of Laboratory Medicine, The Affiliated Wuxi People's Hospital of Nanjing Medical University, Wuxi People's Hospital, Wuxi Medical Center, Nanjing Medical University, Wuxi 214023, China

^b Center of Clinical Research, The Affiliated Wuxi People's Hospital of Nanjing Medical University, Wuxi People's Hospital, Wuxi Medical Center, Nanjing Medical University, Wuxi 214023, China

^c Department of Nuclear Medicine, T Center of Clinical Research, The Affiliated Wuxi People's Hospital of Nanjing Medical University, Wuxi People's Hospital, Wuxi Medical Center, Nanjing Medical University, Wuxi 214023, China

ARTICLE INFO

Keywords:

Glioblastoma
TMZ resistance
CCBE1
Hyper-angiogenesis

ABSTRACT

Acquisition of resistance to temozolomide (TMZ) poses a significant challenge in glioblastoma (GBM) therapy. Neovascularization, a pivotal process in tumorigenesis and development, remains poorly understood in its contribution to chemoresistance in GBMs. This study unveils aberrant vascular networks within TMZ-resistant (TMZ-R) GBM tissues and identifies the extracellular matrix (ECM) protein CCBE1 as a potential mediator. Through *in vivo* and *in vitro* experiments involving gain and loss of function assessments, we demonstrate that high expression of CCBE1 promotes hyper-angiogenesis and orchestrates partial endothelial-to-mesenchymal transition (EndMT) in human microvascular endothelial cells (HCMEC/d3) within GBM. This is likely driven by VEGFC/Rho signaling. Intriguingly, CCBE1 overexpression substantially fails to promote tumor growth, but endows resistance to GBM cells in a vascular endothelial cell-dependent manner. Mechanically, the constitutive phosphorylation of SP1 at Ser101 drives the upregulation of CCBE1 transcription in TMZ resistant tumors, and the excretion of CCBE1 depends on caveolae associated protein 1 (CAVIN1) binding and assembling. Tumor cells derived CCBE1 promotes VEGFC maturation, activates VEGFR2/VEGFR3/Rho signaling in vascular endothelial cells, and ultimately results in hyper-angiogenesis in TMZ-R tumors. Collectively, the current study uncovers the cellular and molecular basis of abnormal angiogenesis in a chemo resistant microenvironment, implying that curbing CCBE1 is key to reversing TMZ resistance.

1. Introduction

Glioblastoma (GBM) is the most prevalent and aggressive malignant brain tumor characterized by sustained neovascularization [1,2]. Chemoresistance is a great challenge for GBM treatment failure, which results in recurrence [3]. Accumulating evidence indicates that adaptive changes in tumor vasculature during chemotherapy provides favorable conditions for the occurrence and development of chemoresistance [4, 5]. Hence, clarifying the intrinsic cellular and molecular mechanisms of abnormal angiogenesis that mediates chemoresistance is of great significance for GBM intervention.

Temozolomide (TMZ) is the first-line chemotherapy reagent for GBM treatment. Resistance in brain tumors is a multifaceted phenomenon that involves intricate interactions and feedback among different levels of biological complexity, including molecular networks, cellular interactions, microenvironmental factors and tissue vasculature [6]. Adaptive alterations of tumor vasculature, such as increased vessel density or altered vessel functionality, affect the chemotherapy response [7]. It is necessary to focus on the dynamic adaptive mechanism of angiogenesis and how it evolves during the intervention response.

Intratumoral angiogenesis refers to the process by which neovascularization occurs from a preexisting vascular network to supply

* Corresponding author. Department of Laboratory Medicine, The Affiliated Wuxi People's Hospital of Nanjing Medical University, 299 Qingyang Road, Wuxi, 214023, China.

E-mail address: zoujan@njmu.edu.cn (J. Zou).

¹ Equal contributors.

nutrients and oxygen to a growing tumor and influence the drug responsiveness [8–10]. Vascular endothelial growth factors (VEGFs) and their receptors (VEGFRs) are the key inducers of angiogenesis in cancers, known to activate survival pathways and promote chemoresistance [11]. Among the VEGFs, a high level of VEGFC specifically has been shown to confer chemotherapy resistance in gastric cancer cells by enhancing Bcl-2 expression [12], and in acute myeloid leukemia through an endothelin-1-dependent induction of cyclooxygenase-2 (COX-2) [13]. However, whether VEGFC is involved in resistance to TMZ and the associated mechanisms remains to be clarified.

In the present study, we observed increased aberrant vascular networks in TMZ-resistant tumors and identified the potential mediator CCBE1, which promotes TMZ-resistance in a vascular endothelial cell-dependent manner. Mechanically, SP1 phosphorylation at Ser101 drives CCBE1 transcriptional upregulation in TMZ resistant tumors, and the excretion of CCBE1 depends on caveolae associated protein 1 (CAVIN1) binding and assembling. CCBE1 is involved in VEGFC processing and maturation, and results in hyper-angiogenesis via VEGFR2/VEGFR3/Rho signaling in TMZ-R tumors. These results provide new insights and novel targets for improving the chemotherapeutic efficacy of TMZ against GBMs.

2. Materials and methods

2.1. Cell culture

The TMZ-S (TMZ-sensitive) and TMZ-R (TMZ-resistant) cells were obtained from TMZ resistant U87 xenografts as previously described [14]. The human brain microvascular endothelial cell line HCMEC/d3 was procured from iCellbioscience Company (iCell-h070), human 293 T and GBM cell lines U87 and LN229 were obtained from the Cell Bank of Type Culture Collection of the Chinese Academy of Sciences (CBTCCAS) and all cell lines were cultured in DMEM (Hyclone) supplemented with 10 % fetal bovine serum (Biological Industries) and 1 % penicillin-streptomycin solution (P/S; Hyclone).

2.2. Vector construction and transduction

Full-length cDNA encoding human *CCBE1*, *SP1* and *CAVIN1* were amplified by PCR and verified by DNA sequencing. The confirmed *CCBE1* cDNA was inserted into a lentivirus vector, pCDH-CMV-EF1a-CopGFP-T2A-Puro with a 3 × Flag at C-terminus. *SP1* lentivirus was constructed by inserting cDNA into lentivirus vector plenti-GFP-Puro. *SP1* non-phosphorylation mutant (S101A) was constructed based on wild-type *SP1* lentivirus with amino acid mutation to alanine at Ser101. *CAVIN1* lentivirus was constructed using lentivirus pLV3-CMV-CoGFP-Puro. All vectors were provided by MiaoLing Plasmid Sharing Platform (Wuhan, China). To obtain stable cell expression of *CCBE1*, *SP1* or *CAVIN1*, the indicated cells were transduced with the established lentivirus or the corresponding construct (Mock), followed by selection with 2 µg/mL puromycin (Sangon Biotech, Shanghai, China).

The short hairpin RNA (shRNA) targeting *CCBE1* and *CAVIN1* were inserted into lentiviral vector pLKO.1-GFP-puro and pLKO.1-mcherry-puro (Beijing Tsingke Biotech Co., Ltd.), respectively. The small interfering RNA (siRNA) sequences targeting human *SP1* were obtained from Genechem Technology (Shanghai, China) and the scramble siRNAs served as negative control (NC). The sequences of shRNA and siRNA are listed in Table S3. For siRNA transfection, cells were transfected with siRNA duplexes using Lipofectamine RNAiMAX transfection reagent (Invitrogen, Carlsbad, CA, USA). Cells were collected for the following assays after 48 h of transfection.

2.3. GBM xenografts in nude mice

Six week-old male BALB/c nude mice were purchased from the Changzhou Cavens Experimental Animal Co., Ltd (Jiangsu, China) and

maintained under specific pathogen-free conditions. To objectively evaluate the degree of neovascularization, and to rule out the interference derived from tumor growth time and tumor size, 5×10^6 TMZ-S cells and 1×10^6 TMZ-R cells (obtained by pre-experiment) were injected subcutaneously into two flanks of each mouse respectively, and isometric tumors derived from same mouse were selected for blood vessel analysis. The tumors were collected at about 800–1000 mm³ for follow-up experiments. For TMZ sensitivity assay, the indicated cells were transferred into 100 µL of DMEM: Matrigel (8:1, v/v) were injected s. c. Into the flank of each nude mouse, and tumors were allowed to develop until a volume of 100–150 mm³ was reached. Mice were then randomized to receive oral saline, TMZ (20 mg/kg) or Pazopanib (100 mg/kg) once every other day for 12–14 days. Tumor sizes were measured every 2 days post-first treatment and tumor tissues were collected at the end point for tumor weight measurement. All animal procedures were performed in accordance with the National Institutes of Health's Guide for the Care and Use of Laboratory Animals.

2.4. HCMEC tube formation assay

The Matrigel matrix was thawed overnight at 4 °C and subsequently added into a pre-cooled 48-well plate at a volume of 100 µL per well, followed by incubation at 37 °C for 30 min to allow for solidification. HCMEC cells were then digested and resuspended in culture medium from the indicated cells which have cultured for 48 h, 4×10^4 cells were then seeded onto the Matrigel-coated 48-well plate. Following 16–20 h of culture, images were captured either directly or after staining with calcein (1 µL/well) for 20 min. Three replicates were performed for each group, and five random visual fields were selected. The number and length of formed tubes were analyzed using ImageJ software.

2.5. 3D cell invasion assay

A three-dimensional (3D) cell culture chip (AIM Biotech) was utilized to determine the degree of cell invasion. Type I rat tail collagen (Gibco) was prepared at a concentration of 2.5 mg/mL, which was then diluted with 10 × PBS. The stiffness of the gel was adjusted by controlling the pH to 11 using 0.5 M NaOH. The preparation process was conducted on ice and all reagents were pre-cooled. The prepared hydrogel was added into the middle gel channel and allowed to gel at 37 °C for 30 min. HCMEC cells co-cultured with the indicated GBM cells were collected and suspended in FBS-free DMEM. The cell concentration was adjusted to 2.0×10^6 /mL, and 20 µL of the cell suspension was added into the left cell culture channel. The indicated cell culture medium mixed with DMEM containing 20 % FBS was added into the right gel channel. The device was placed diagonally at 37 °C to facilitate the attachment of the cells onto the collagen scaffold by gravity. The cell invasion was observed and photographed at different time points with an EVOS living cell imager system (EVOS FL Auto, Life Technologies), and the calculation was performed using ImageJ software.

2.6. Cell growth assay and EdU incorporation assay

In the cell growth assay, a total of 5×10^4 cells were seeded into 12-well plates and cultured with CM from TMZ-S/TMZ-R cells or TMZ-R NC/CCBE1 KD cells and counted at the indicated time points. EdU incorporation assay was performed to detect DNA replication and cell multiplication. Briefly, 2×10^4 cells were seeded on poly-L-lysine (Sigma-Aldrich) coated coverslips in 24-well plates co-cultured with or without HCMECs for 24 h, subsequently added 10 µM EdU (Keygen Biotech) and continued cultivation for 12 h. Then cells were fixed with 4 % paraformaldehyde (PFA) for 30 min and following staining procedure was performed according to the manufacturer's instructions (Click-iT EdU, Keygen Biotech). Hoechst 33,342 (Thermo) were used to stain nuclei. The percentage of EdU⁺ positive cells were out of the total number of cells (labeled with Hoechst) was calculated.

2.7. Dox cellular uptake assay

GBM/HCMEC co-cultures were established in a 6-well cell insertion plate (0.4 µm, BIOFIL) and incubated for 24 h. Next, the HCMEC cells in the upper chamber, separated by a 0.4 µm membrane, were removed. To the wells containing GBM cells, either 10 µL Doxorubicin (DOX, 5 µM) or DMSO (control) was added. After 1 h, cells were collected for flow cytometry analysis. The number of cells exhibiting fluorescence, indicating DOX uptake, was quantified using FlowJo software to assess drug resistance and uptake ability.

2.8. H&E, immunohistochemistry (IHC) and immunofluorescence (IF) staining

Histological and immunological analyses were conducted following previously established protocols [15]. For immunohistochemistry (IHC) and immunofluorescence (IF) staining, primary antibodies including CD31 (1:200), CCBE1 (1:100), α-SMA (1:200), VE-cadherin (1:300), Rho (1:300), γ-H2AX (1:200) were employed. The proportion of CD31/CCBE1 positive cells relative to the total number of cells in five randomly selected fields was calculated using ImageJ software.

2.9. RT-qPCR assay

Cell or tissue RNA was extracted using the Cell/Tissue Total RNA Isolation Kit (Vazyme). For reverse transcription-quantitative polymerase chain reaction (RT-qPCR), HiScript III RT SuperMix for qPCR (Vazyme) was used to reverse-transcribe RNA to cDNA. Universal SYBR qPCR Master Mix (Vazyme) was used for qPCR. The primer sequences used were specified in Table S1.

2.10. Immunoblot (IB) analysis

Cell or tissue protein was extracted using RIPA Lysis Buffer (Cell Signal Technology). For the cell supernatant, cell culture medium was collected and transferred to AMICON ULTRA-15 (Millipore) and concentrated solution were obtained by centrifugation (4000 rpm) at 4 °C for 25 min for 3–4 times. Then the cellular super-albumin was obtained using liquid sample total protein extraction reagent (APPLYGEN). For the TMZ treatment assay, cells were treated with 200 µM TMZ for 48 h to detect the protein level of CCBE1 in cell lysate and supernatant. All samples diluted in loading buffer, denatured by heating at 98 °C for 10 min then loaded onto prepared SDS-PAGE gel for subsequent immunoblot analysis.

2.11. ELISA assay for VEGFC and his-tag

The indicated cell culture medium was collected for ELISA analysis. Solutions were centrifuged at 300 g for 10 min to remove cell precipitate. VEGFC was detected by VEGFC ELISA kit (MULTI SCIENCES) or His Tag ELISA Detection Kit (Genscript) according to the manufacturer's instructions. To monitor the processing and maturation of VEGFC, a VEGFC vector containing a His tag incorporated at the N-terminus domain (NTD) was constructed based on pCMV-GST-Puro plasmid (His-VEGFC) (Fig. S7A). As shown in the diagram, the detection of His can evaluate the maturity of VEGFC.

2.12. Luciferase reporter assay

The CCBE1 promoter was obtained on Ensembl (<http://www.ensembl.org/index.html>). SP1 binding sites on the CCBE1 promoter region were analyzed through JASPAR (<http://jaspardev.genereg.net/>) and ALGGEN-PROMO (<https://alggen.lsi.upc.es/>) databases. To evaluate SP1 transcriptional activity on CCBE1, the promoter region of CCBE1 was cloned into pGL3-Luc basic reporter vector (Promega) constructed by MiaoLing plasmid platform, hereby referred to as pCCBE1-

Luc-WT. SP1 binding site mutant plasmids were constructed based on WT. Indicated cells were transfected with the established vectors for 48 h and were harvested for detection. pRL-TKRenilla luciferase plasmid (Promega) served as a transfection control. Renilla and luciferase signals were detected using the Dual-Luciferase® Reporter Assay System (Promega).

2.13. Chromatin immunoprecipitation (ChIP)-qPCR assay

Chromatin immunoprecipitation (ChIP) assay was performed by a Simple ChIP Enzymatic Chromatin IP Kit (CST) according to the manufacturer's instructions. Briefly, 2×10^7 TMZ-S or TMZ-R cells and 5 µg anti-SP1 antibodies were used for each ChIP. Anti-IgG and anti-Histone H3 antibodies were used as negative and positive controls, respectively. ChIP-derived DNA was quantified by qRT-PCR. The primers for ChIP-qPCR were designed according to the three putative SP1-binding sites in the CCBE1 promoter (Fig. 3J). The primers are listed in Table S2. ChIP efficiency was expressed according to our previously established method [16].

2.14. Immunoprecipitation (IP) and mass spectrometry (MS) assay

Cell lysates were extracted using RIPA Lysis Buffer (CST), and precipitated using anti-Flag magnetic beads (MBL Life Sciences, Nagoya, Japan). Precipitated products were analyzed by Western blot using CCBE1 antibody to confirm the presence of the target protein. Precipitated products were washed and separated by SDS-PAGE gel. The integrated electrophoretic bands were cut off and subjected to in-gel digestion with trypsin (Gibco). The derived peptides were filtered and solubilized with a Loading Buffer. The solubilized peptides were analyzed and identified by LC-MS/MS on a mass spectrometer (Hangzhou Lc-Bio Technologies, China) to identify proteins bound to CCBE1.

2.15. Online cancer database resources and analysis

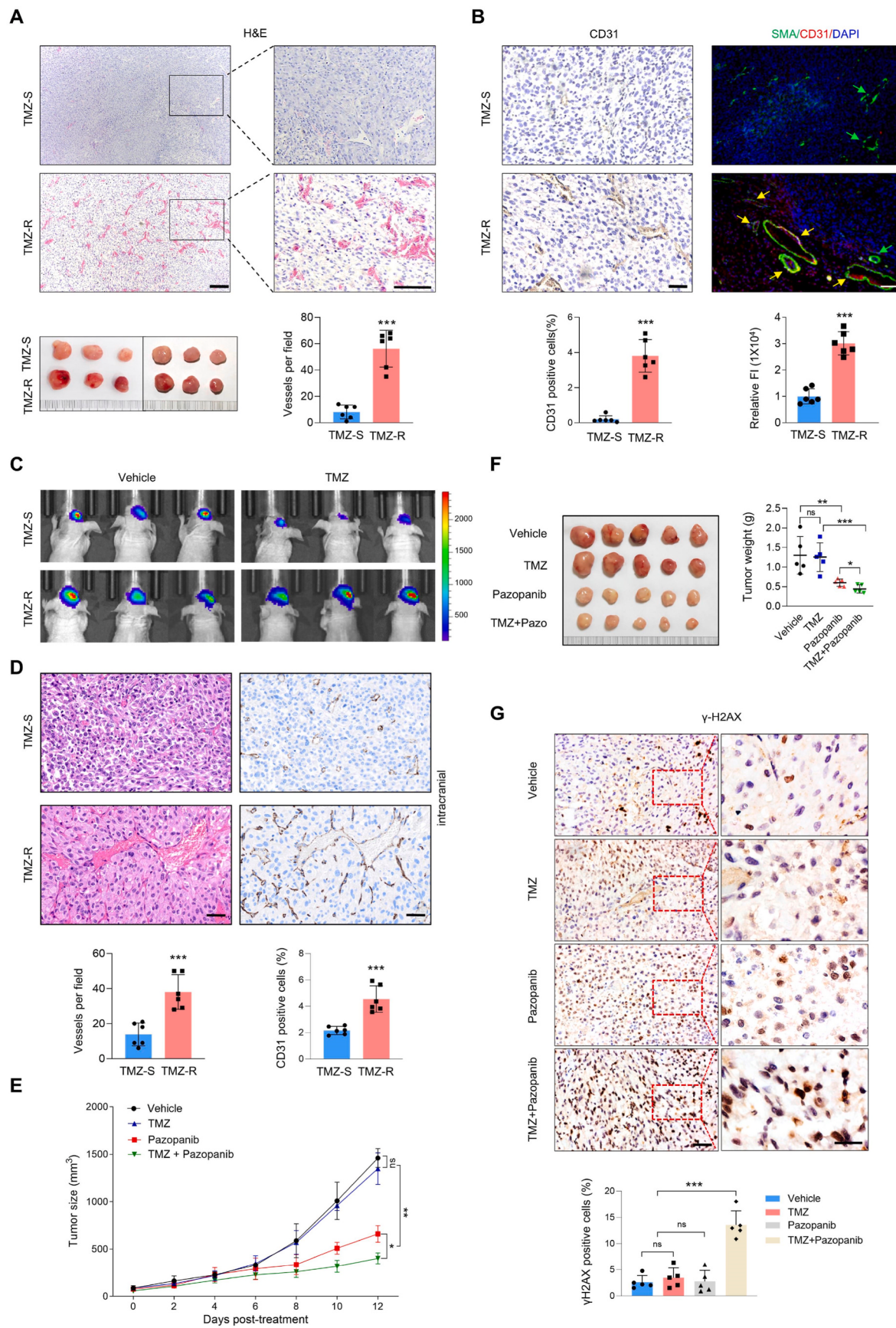
For Kaplan-Meier analysis of survival, GBM data with chemotherapy/no chemotherapy information were derived from the CGGA mRNASeq-325 and mRNASeq-693 dataset (<http://www.cgga.org.cn/>), TCGA-GBM HG-U133A dataset (<http://glouis.bioinfo.cnio.es/>) and TCGA GBM- Affymetrix Human Exon 1.0 ST dataset (<https://betastasis.com/gliona/tcgab/>). HALLMARK_ANGIogenesis and KESHELA-VA_MULTIPLE_DRUG_RESISTANCE gene sets were downloaded from the Molecular Signature Database v7.5.1 (H: Hallmark gene sets and C2 curated gene sets) (<https://www.gsea-msigdb.org/gsea/msigdb>). The 'Gene Set Variation Analysis (GSVA)' package [17] was used for single-sample gene set enrichment analysis (ssGSEA) to evaluate the enrichment score of each tumor sample in each of the GBM datasets. The optimal cutoff point was determined using X-tile software.

For Pearson correlation analysis, KMDR score and Angiogenesis score were analyzed in CGGA mRNASeq-325, CGGA mRNASeq-693, and TCGA-GBM HG-U133A datasets. KDR, FLT4, FLT1 and MDR1 gene expression data were obtained from online TCGA-GBM Cell 2013 (cBioPortal: <https://www.cbioportal.org/>), CGGA mRNASeq-325/693, and Gravendeel-GBM datasets (<http://glouis.bioinfo.cnio.es/>).

For gene expression analysis (Fig. S4), CCBE1 expression data were obtained from the CGGA mRNASeq-693 dataset with the primary and recurrence information. The obtained data were analyzed using GraphPad Prism 8.0 software.

2.16. RNA sequencing data analysis

TMZ-S/R tumor RNA sequencing was performed by Yike Health Research Institute, and the differentially expressed genes (DEGs) were obtained. Next, "ggplot 2" package was used to visualize a heat map of the upregulated DEGs with a value of log 2 fold change ($|\log_{2}FC| > 10$ as well as $P. adj < 0.05$ in TMZ-R tissues (<https://www.xiantaozi.com/>)). In



(caption on next page)

Fig. 1. Hyper-angiogenesis contributes to chemoresistance in GBM. **A.** Representative images of derived-tumor sections stained with H&E showing vessel distribution (upper panel). The lower panel shows the tumors and the quantification of vessels per field ($n = 6$, *** $p < 0.001$). Bars, 200 μ m. **B.** Representative images of immunohistochemical (IHC) and CD31/α-SMA double immunofluorescence (IF) staining of tumor sections. The lower panel shows the quantification of CD31 positive cells and CD31/α-SMA double positive vessels ($n = 6$, *** $p < 0.001$). Bars, 50 μ m. **C.** Bioluminescent images of intracranial xenografts derived from TMZ-S and TMZ-R cells ($n = 6$). **D.** Representative H&E staining of locally enlarged images derived from intracranial xenografts tumors (Left) and Representative images of CD31 IHC of derived intracranial xenografts tumors (Right). Bars, 50 μ m. **E.** Tumor growth assay of TMZ-R derived xenografts receiving indicated treatment every two days after tumors reaching 150 mm³ ($n = 5$; ns, no significance, * $p < 0.05$, ** $p < 0.01$). **F.** Representative images of xenografts collected at the final day (left) and the quantification of tumor weight (right; $n = 5$, ** $p < 0.01$, *** $p < 0.001$). **G.** Representative images of γH2AX IHC staining and quantification (right; $n = 5$, *** $p < 0.001$). Bars, 200 μ m.

order to investigate functions of the upregulated DEGs ($(|\log_{2}FC|) > 1$, P-adj < 0.05) in TMZ-R tumors, the Gene Ontology (GO) enrichment analysis was performed online (<https://www.webgestalt.org/>).

2.17. Statistical analysis

All experiments were repeated at least three times to ensure statistical validity. Data were expressed as mean \pm standard deviation (SD), and analyzed using GraphPad Prism 8.0 software. The statistical differences between two groups was determined by the Student's t-test. A p-value of less than 0.05 was considered statistically significant.

3. Results

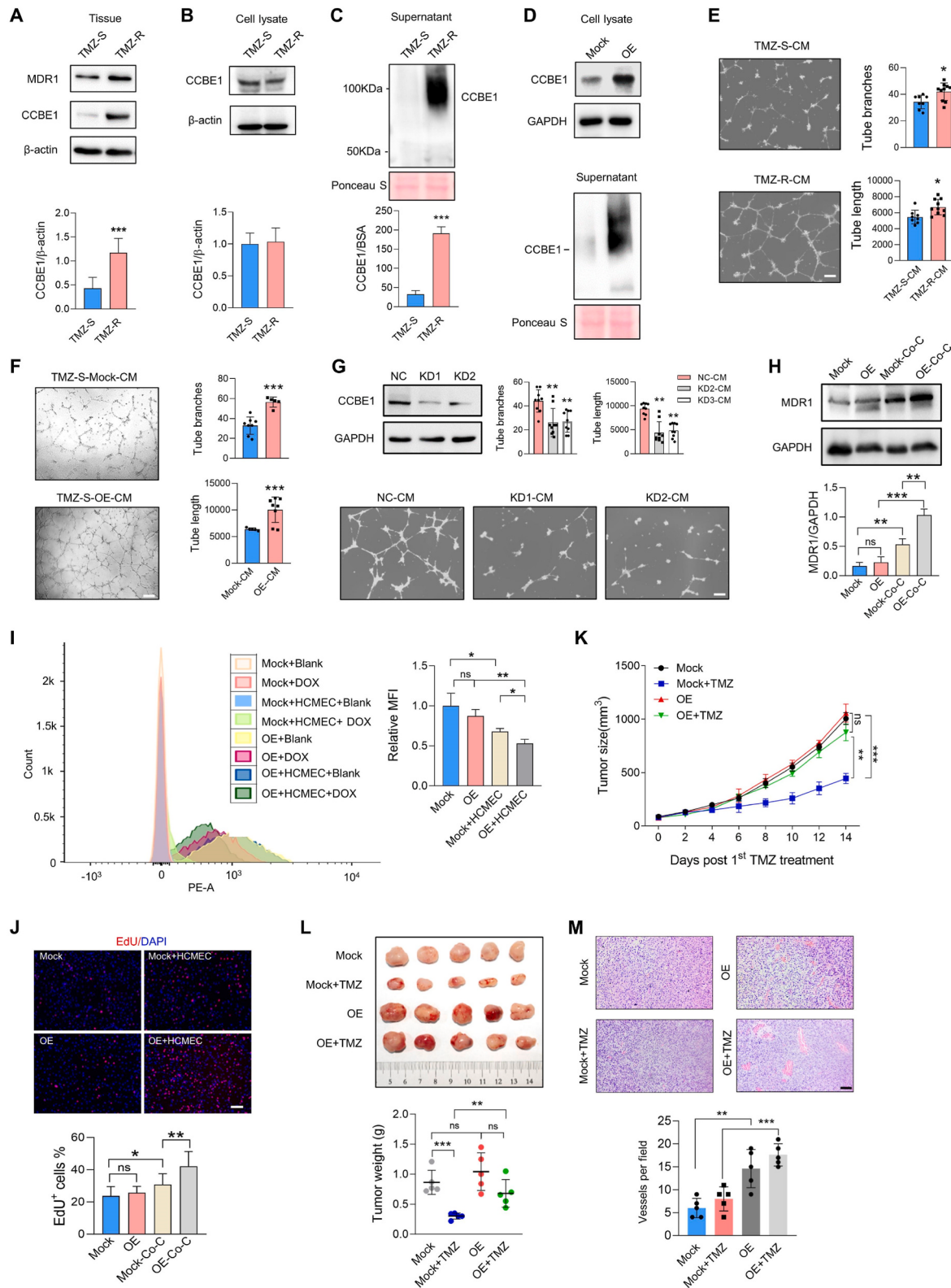
3.1. Hyper-angiogenesis contributes to chemoresistance in GBM

The association between angiogenesis and chemotherapy outcomes in GBM was analyzed using online clinical data. As shown in Figs. S1A and S1B, patients with higher HALLMARK_ANGIOGENESIS scores according to gene set enrichment analysis (GSEA) of a combined CGGA-GBM dataset and TCGA-GBM-HG U133A database observed poorer survival outcomes when receiving chemotherapy. A positive correlation between the ssGSEA enrichment score of HALLMARK_ANGIOGENESIS (Angiogenesis score) and LABIOMULTIPLEX

DRUG_RESISTANCE (KMDR) gene sets scores in the CGGA and TCGA GBM datasets suggested a link between angiogenesis and chemoresistance in GBM (Fig. S1C). Additional vascular markers, such as vascular endothelial growth factor receptor family members KDR (VEGFR2) and FLT1 (VEGFR1) were positively associated with MDR1 (ABCB1) (Fig. S2), the multidrug resistance associated gene [18], suggesting angiogenesis in tumors is closely linked to chemosensitivity. Next, in our established *in vivo* TMZ-resistance model [14], a significant enrichment of disordered blood vessels was observed in TMZ-resistant tissues (TMZ-R) as compared with TMZ-sensitive tissues (TMZ-S) (Fig. 1A). CD31 (PECAM1), an endothelial cell marker, was further selected as an indicator of vascular abundance [19]. The analysis of CD31 positive cells by immunohistochemistry (IHC) and double immunofluorescence (IF) staining of CD31 and the pericyte marker α-smooth muscle actin (α-SMA) further indicated the increased neovascularization in TMZ-R tumors (Fig. 1B), strengthening the association between angiogenesis and chemoresistance. In addition, the results derived from intracranial implantations also indicated that tumors derived from TMZ-R cells contained TMZ-resistant qualities (Fig. 1C), including greater vascularization (Fig. 1D). To assess the role of angiogenesis in mediating TMZ-resistance, a novel angiogenesis inhibitor, Pazopanib was applied in the subsequent *in vivo* study [20]. TMZ-R tumors exhibited no response to TMZ therapy, while Pazopanib introduction resulted in a significant growth inhibition and TMZ sensitivity (Fig. 1E and F). Moreover, tumors receiving Pazopanib developed less blood vessels (Fig. S3) and resumed TMZ-induced DNA damage as indicated by phosphorylated Histone H2A.X (Fig. 1G). Collectively, these data suggest that increased vasculature upon chemotherapy predicts poor outcomes for GBM patients, and that anti-angiogenesis is a potential solution for reversing chemoresistance.

3.2. CCBE1 upregulation drives TMZ-resistance by promoting angiogenesis

To explore the mechanism underlying abnormal angiogenesis in TMZ-resistant tissues, RNA sequencing (RNA-Seq) was performed in TMZ-S and TMZ-R tumors to identify de-regulated genes (DEGs). It revealed 1721 upregulated genes and 697 downregulated genes in TMZ-R tumors according to the threshold of $\log_2FC > 1$. The top DEGs with $\log_2FC > 10$ are shown in hierarchical clustering (Fig. S4A). GO BP pathway analysis indicated that upregulated DEGs were enriched in acid secretion, cell-cell adhesion, regulation of inflammatory response, angiogenesis, positive regulation of cytokine production, extracellular structure organization and leukocyte regulation (Fig. S4B). Among those upregulated genes in TMZ-R, CCBE1 (Fig. S4C), functioning in extracellular matrix remodeling and migration, is closely linked to (lymph) angiogenesis [21,22] and acts as a potential therapeutic target for chemotherapy [23]. Evidence from bioinformatics analysis indicated that CCBE1 was upregulated in recurrent GBMs (Fig. S4D) and was a predictor of poor outcomes for GBM patients receiving chemotherapy (Fig. S4E). Ample evidences suggest that the expression of ATP-binding cassette (ABC) transporters can confer resistance to cytotoxic and targeted chemotherapy, particularly MDR1 (ABCB1) [18]. The correlation analysis demonstrated that CCBE1 expression in GBM was positively associated with MDR1 expression, and negligibly correlated with ABCC3 (Fig. S4F). CCBE1 protein was confirmed to be upregulated in TMZ-R tissues (Fig. 2A) though no difference was detected at the intracellular level (Fig. 2B). CCBE1 was identified as an extracellular protein significantly increased in cell supernatant derived from TMZ-R cells (Fig. 2C). An increase of MDR1 in TMZ-R tissues (Fig. 2A) was also observed, implying a role in the regulation of drug uptake. The characteristic of CCBE1 as a secreted protein was further demonstrated in TMZ-S cells expression ectopic CCBE1 (Fig. 2D). Subsequent experiments (Fig. 2E; Figs. S5A–B) showed the promotion of TMZ-R-derived supernatant on tube formation, proliferation, and invasion of HCMEC cells, a human cardiac microvascular endothelial cell line. Accordingly, supernatant derived from TMZ-S cells expressing ectopic CCBE1 markedly increased the tube formation of HCMECs (Fig. 2F), and CCBE1 knockdown (KD) significantly impaired the promotion of tube formation of supernatant derived from TMZ-R cells (Fig. 2G). Additional functional experiments indicated the promotion of CCBE1 on cell proliferation and invasion of HCMECs (Figs. S5C and D). Interestingly, the expression of MDR1 in TMZ-S cells were not affected by CCBE1 overexpression, while a significant increase was observed in cells co-cultured with HCMECs. CCBE1-overexpressing cells achieved highest MDR1 expression (Fig. 2H). Next, DOX was used to determine whether MDR1 upregulation induced by CCBE1 with the aids of HCMECs resulted in drug accumulation impairment in TMZ-S cells. Flow cytometry assay showed that the uptake of DOX by TMZ-S cells was decreased upon co-culture with HCMECs, and CCBE1 overexpression further enhanced this inhibition (Fig. 2I), indicating drug uptake inhibition induced by CCBE1 depends on the aids of HCMECs. Correspondingly, CCBE1 overexpression aggravated TMZ-resistance of TMZ-S cells induced by HCMEC co-culture, as indicated by the number of replicating cells (Fig. 2J). The *in vivo* study indicated that the growth of Mock tumors was significantly inhibited by TMZ, while tumors derived from TMZ-S expressing ectopic CCBE1 contained comparable growth capacity to



(caption on next page)

Fig. 2. Upregulation of CCBE1 drives TMZ-resistance via promoting angiogenesis. **A.** Immunoblot (IB) analysis shows MDR1 and CCBE1 upregulation in TMZ-R tumors. β -Actin served as a loading control ($n = 4$, *** $p < 0.001$). **B.** IB assay indicates the expression of CCBE1 in cells derived from indicated tumors ($n = 3$). **C.** IB analysis detects CCBE1 expression in the supernatant from indicated cells ($n = 3$, *** $p < 0.001$). Ponceau S staining shows bands at 70 kDa, serving as a loading control of supernatant samples. **D.** IB analysis of CCBE1 in the cell lysate and supernatant (lower panel) of U87 cells expressing Mock or ectopic CCBE1. GAPDH and Ponceau S staining served as a loading control of cell lysate and supernatant samples, respectively. **E.** Tube formation of HCMECs incubated with conditioned medium (CM) from TMZ-S/TMZ-R cells. Tube formation was defined by the number of tube branches and tube length ($n = 6$, * $p < 0.05$). Bars, 100 μ m. **F.** Tube formation of HCMECs incubated with CM from TMZ-S expressing Mock or ectopic CCBE1 ($n = 6$, *** $p < 0.001$). Bars, 100 μ m. **G.** Tube formation of HCMECs incubated with CM from TMZ-R cells with CCBE1 knockdown ($n = 6$, ** $p < 0.01$). IB assay confirms the expressing of CCBE1 in TMZ-R cells with CCBE1 knockdown. Bars, 100 μ m. **H.** IB analysis of MDR1 expression in indicated TMZ-S cells with or without HCMECs coculture ($n = 3$, ** $p < 0.01$, *** $p < 0.001$). **I.** Flow cytometry assay (left) and statistical analysis of mean fluorescence intensity (MFI; right) show the DOX uptake by the indicated cells ($n = 3$, * $p < 0.05$, ** $p < 0.01$). **J.** EdU incorporation assay detects the proliferation of indicated cells with or without HCMECs coculture ($n = 9$, * $p < 0.05$, ** $p < 0.01$). Bars, 100 μ m. **K.** Tumor growth assay of xenografts derived from indicated TMZ-S cells received indicated treatment every two days after tumors reached 150 mm³ ($n = 5$, ** $p < 0.01$, *** $p < 0.001$). **L.** Representative images of xenografts collected at the final day (left) and tumor weight quantification (right; $n = 5$, ** $p < 0.01$, *** $p < 0.001$). **M.** Representative images of derived-tumor sections stained with H&E (upper panel). The lower panel shows the quantification of vessels per field ($n = 5$, ** $p < 0.01$, *** $p < 0.001$). Bars, 200 μ m.

Mock expressing tumors, even those receiving TMZ treatment (Fig. 2K and L), and CCBE1 overexpressed tumors exhibited more abundant blood vessels compared the Mock ones with or without TMZ treatment (Fig. 2M). Accordingly, CCBE1 knockdown failed to affect TMZ-R tumor growth in the absence of TMZ, while upon TMZ treatment, it resulted in a significant promotion of chemosensitivity (Fig. S6). Therefore, these data support that CCBE1 upregulation is a key event driving GBM chemoresistance via impairment of drug uptake of tumor cells, likely mediated by induced angiogenesis.

3.3. Chemotherapy drives SP1 phosphorylation and CCBE1 transcriptional upregulation

To explore the potential mechanism underlying CCBE1 upregulation in TMZ-R, the -1000 upstream region from the translation start site of CCBE1 was analyzed to predict putative binding sites of transcription factors (TFs). Three binding sites for SP1 were identified (Specificity protein 1) in the upstream region of the CCBE1 promoter (Fig. 3A). SP1 is a transcriptional regulator involved in cellular differentiation and growth, apoptosis, immune responses, and DNA damage. SP1 was found to be significantly activated in TMZ-resistant tumors, as reflected by phosphorylation, which determines the activity of SP1 [24] (Fig. 3B). Accordingly, SP1 knockdown mediated by siRNA decreased CCBE1 expression in U87 and LN229 cells (Fig. 3C). Moreover, using the selective SP1 inhibitor Plicamycin A (Mithramycin A, MITA), resulted in a decrease of CCBE1 expression in U87 and LN229 cells (Fig. 3D), confirming SP1 as an upstream regulator of CCBE1. To determine whether SP1 directly regulated CCBE1 transcription in GBM cells, a CCBE1 reporter vector containing the -1000 upstream region from the translation start site was established. It showed that the luciferase activity of CCBE1 promoter was greatly increased in TMZ-R cells (Fig. 3E), and that SP1 promoted CCBE1 reporter activity in TMZ-R cells in a dose-dependent manner (Fig. 3F). Notably, mutant reporters according to the putative SP1-binding sites exhibited significantly lower luciferase activity (Fig. 3G). Moreover, ChIP-qPCR assay targeting these putative binding sites provided evidence that SP1 directly binds to the CCBE1 promoter, and that Site 3 recruits more SP1 in TMZ-R (Fig. 3H). It has been well addressed that phosphorylation influences the transcriptional activity of SP1, among which S101 phosphorylation is closely associated with DNA-damage responsive SP1 transcriptional activity [25,26]. Accordingly, SP1 non-phosphorylation mutant (S101A) was constructed to explore whether S101 phosphorylation of SP1 is necessary for CCBE1 transcription. As shown in Fig. 3I, SP1 overexpression resulted in an increase of overall and S101 phosphorylation, as well as an upregulation of CCBE1. However, S101A failed to alter SP1 phosphorylation, and loss of the regulation of CCBE1, which also was reflected in CCBE1 reporter assay (Fig. 3J). Collectively, these results demonstrated that chemotherapy induced SP1 phosphorylation and activity directly promotes CCBE1 expression.

3.4. Chemotherapy induces CAVIN1 binding and CCBE1 secretion

Besides the transcription upregulation, a robust accumulation of CCBE1 in the supernatant of TMZ-R cells additionally suggested that chemotherapy promotes its exocrine function. To identify the key factor that mediates CCBE1 secretion, an IP assay followed by LC/MS-MS analysis was performed. Briefly, U87 cells expressing ectopic Flag-tagged CCBE1 and the binding proteins in cell lysate were enriched by Flag-conjugated magnetic beads (Fig. 4A). A Venn assay screened 69 proteins specifically bound to CCBE1, and CCBE1 got the highest score, confirming the satisfactory specificity of the IP (Fig. 4B). Among the top five CCBE1 binding proteins, CAVIN1 attracted attention due to its involvement in caveolae formation and exosome secretion [27]. The subsequent IP analysis verified the cellular intrinsic binding of CCBE1 and CAVIN1 in U87 cells (Fig. 4C). Moreover, this binding was found to be enhanced in TMZ-R cells (Fig. 4D). An important finding was that TMZ treatment drove more CAVIN1 binding to CCBE1 and subsequent CCBE1 secretion in TMZ-S cells without affecting the expression of CAVIN1 (Fig. 4E). CAVIN1 overexpression in TMZ-S cells resulted in a great increase of CCBE1 secretion even without TMZ treatment, but did not lead to CCBE1 upregulation (Fig. 4F). Accordingly, CAVIN1 knockdown resulted in a significant decrease of CCBE1 enrichment in the supernatant of TMZ-R cells (Fig. 4G). As a result, CAVIN1 overexpressed U87 derived conditioned medium enhanced the tube formation of HCMECs, a phenomenon inhibited by medium derived from cells treated with GW4869, an exosome inhibitor [28] (Fig. 4H). Consistently, conditioned medium from CAVIN1 knockdown TMZ-R cells suppressed the angiogenic ability of HCMECs (Fig. 4I). These data indicated that chemotherapy promotes CCBE1 secretion in a CAVIN1 binding-dependent manner that likely promotes the assembly of exocytosis components in GBM.

3.5. CCBE1 promotes VEGFC/VEGFR/rho signaling and partial EndMT in HCMECs

CCBE1 has been linked to lymphangiogenesis and VEGFC/VEGFR3 signaling [29,30], urging the determination of whether CCBE1-driven angiogenesis in chemosensitive tumors is associated with intensifying VEGFC maturation. Using the VEGFC ELISA kit, it was observed that VEGFC was more enriched in the supernatant derived from TMZ-R cells (Fig. 5A), and that CCBE1 knockdown inhibited VEGFC secretion (Fig. 5B). VEGFC secretion was driven by TMZ treatment, and this increase was impaired by CCBE1 knockdown (Fig. 5C). Moreover, CCBE1 overexpression induced VEGFC maturation in the supernatant of TMZ treated U87 cells (Fig. 5D), resulting in increased secretion of VEGFC (Fig. 5E). To document the function of CCBE1 on VEGFC processing and maturation, we constructed a VEGFC vector containing a His-tag incorporated at N-terminus domain (NTD). As shown in the diagram of the VEGFC structural domain, a change in His content in the cell supernatant represents the splicing and processing of VEGFC (Fig. S7A).

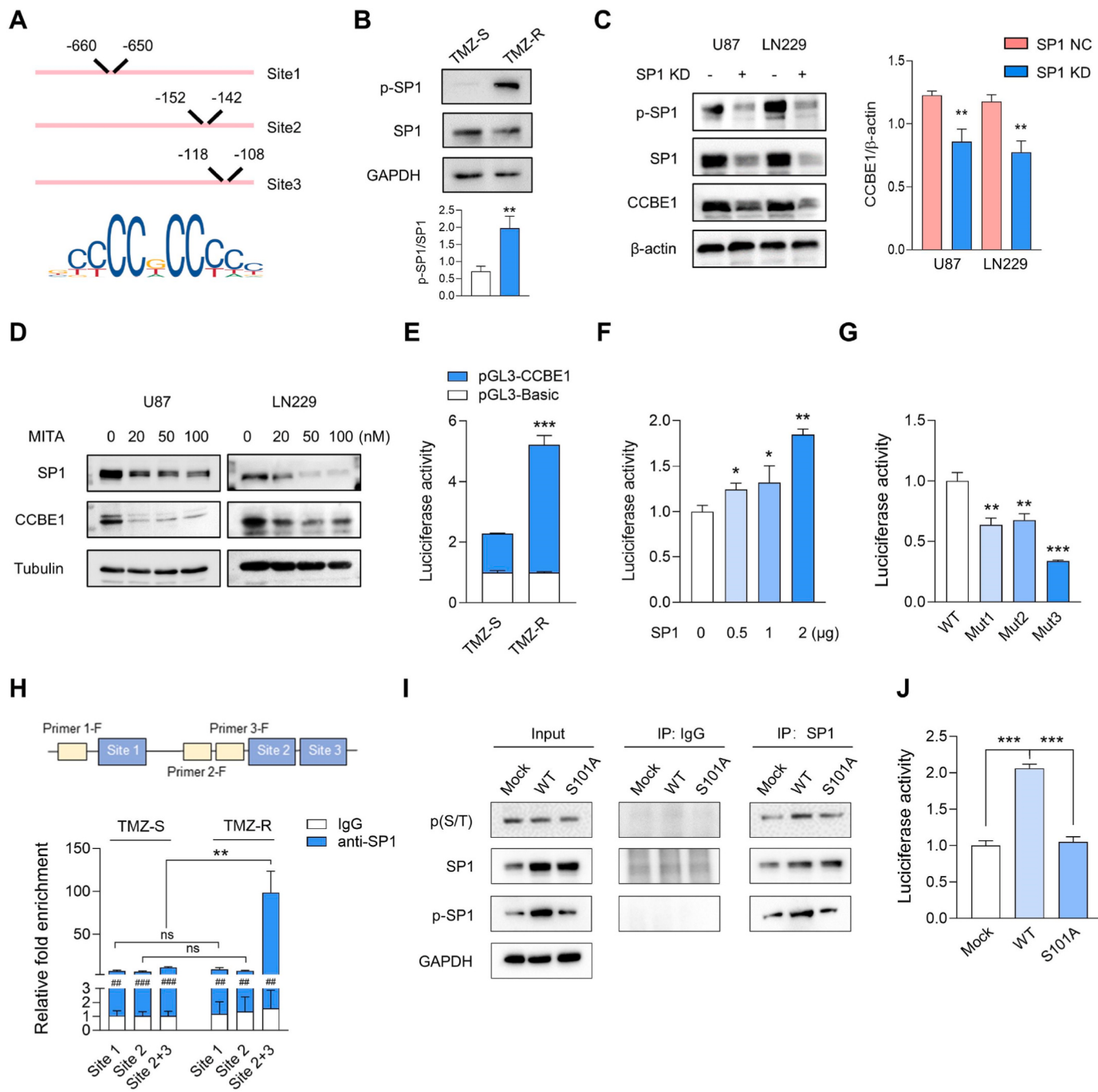


Fig. 3. Chemotherapy-induced SP1 phosphorylation directly results in CCBE1 transcriptional upregulation. **A.** Transcription factor prediction highlights putative SP1 binding sites in the upstream region of the CCBE1 promoter. **B.** IB assay shows the expression of SP1 and its phosphorylation (Ser101) in TMZ-S and TMZ-R cells ($n = 3$, $**p < 0.01$). **C.** IB assay detects CCBE1 alteration in U87 and LN229 cells with or without SP1 knockdown ($n = 3$, $**p < 0.01$). **D.** IB analysis of CCBE1 and SP1 in U87 and LN229 cells treated with Plicamycin A (MITA) for 48 h. Tubulin served as a loading control. **E.** Dual-luciferase assay shows the activity of CCBE1 reporter ($n = 6$, $***p < 0.001$). **F.** Luciferase assay assesses CCBE1 reporter activity in U87 cells expressing ectopic SP1 ($n = 6$, $*p < 0.05$, $**p < 0.01$). **G.** Luciferase assay evaluates CCBE1 reporter activity in U87 cells expressing indicated CCBE1 promoters ($n = 6$, $**p < 0.01$, $***p < 0.001$). Mutations in putative binding sequences were listed. **H.** ChIP-qPCR detects the enrichment of SP1 binding to the promoter of CCBE1 containing indicated mutation in TMZ-S and TMZ-R cells ($n = 6$, $**p < 0.01$, $#p < 0.05$, $##p < 0.01$, $###p < 0.001$ as compared to IgG derived enrichment). The diagram shows the location of primers designing. **I.** IB analysis of SP1 Ser101 and global phospho-serine or threonine phosphorylation (p(S/T)) in U87 cells transduced with wild-type (WT) SP1 and S101A mutant. **J.** Dual-luciferase assay detects CCBE1 reporter activity in U87 cells transduced with the indicated construct ($n = 3$, $***p < 0.001$).

His ELISA assay showed that pro-VEGFC (His-VEGFC) was significantly reduced in supernatants derived from TMZ-R cells, TMZ-treated TMZ-S cells, and CCBE1 overexpressed TMZ-S cells. Moreover, pro-VEGFC (His-VEGFC) was increased in supernatants from TMZ-R cells with CCBE1 KD (Fig. S7B), confirming the effect of CCBE1 on VEGFC maturation. Considering that VEGFC is a secretory protein, the expression of

VEGFC were detected by qPCR, indicating the expression of VEGFC was not affected in indicated samples. Next, whether CCBE1 acts as an upstream regulator for Rho/VEGFR2-VEGFR3 signaling in HCMECs that promoting malignant phenotypes of GBM cells was investigated. The conditioned medium from CCBE1 knockdown expressing TMZ-R cells failed to initiate Rho upregulation and VEGFR2/VEGFR3

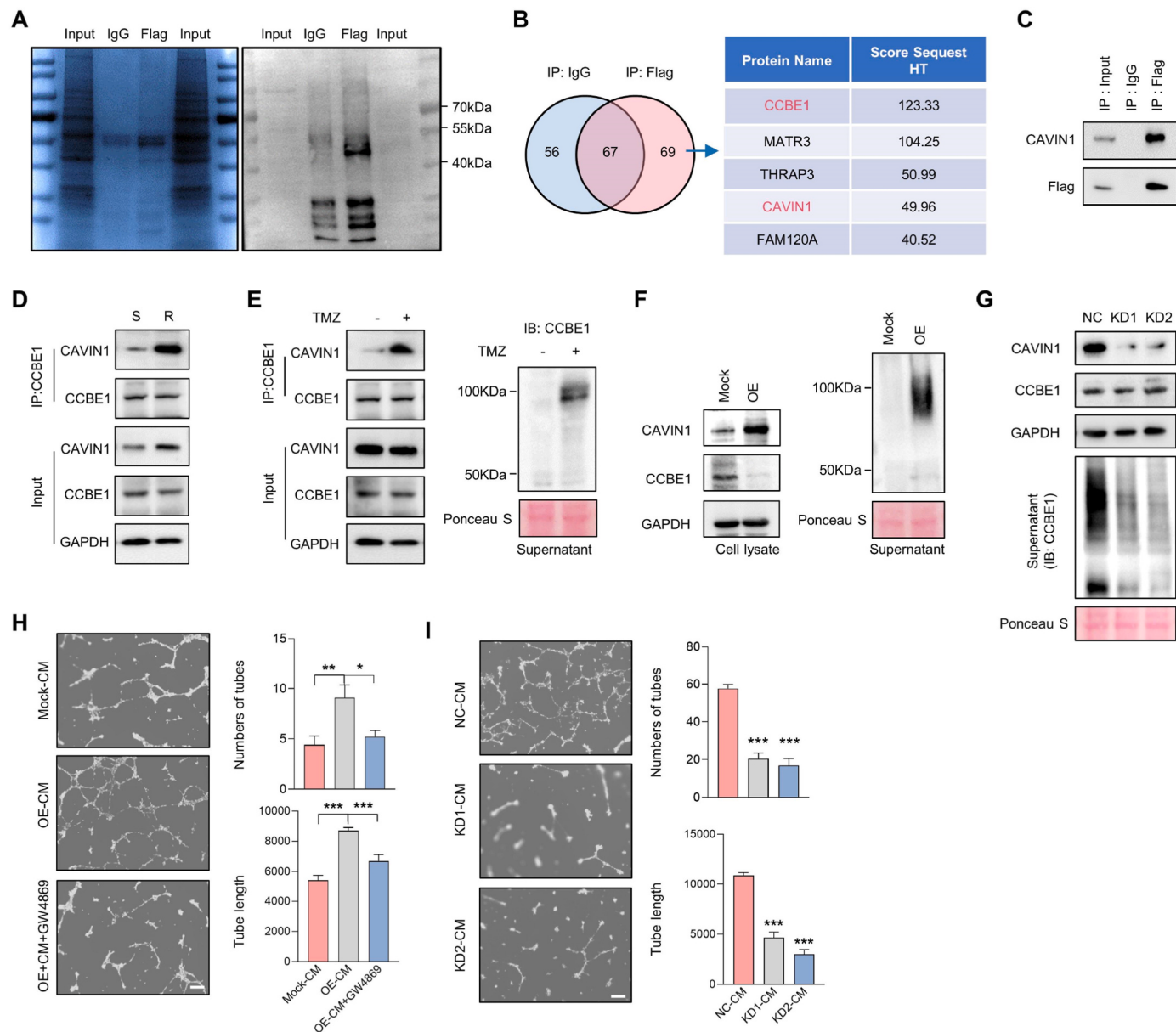


Fig. 4. Chemotherapy-induced CAVIN1 binding and secretion of CCBE1. **A.** Coomassie brilliant blue staining of SDS-PAGE gel (left) and IB analysis (right) showing proteins bound to CCBE1 enriched by Flag antibody-labeled precipitation. **B.** Venn diagram identifying proteins by mass spectrometry sequencing (left) and the top five CCBE-binding proteins (right). **C.** Immunoprecipitation (IP) confirming the interaction between CAVIN1 and CCBE1 in U87 cells. **D.** IP assay detecting the interaction between CCBE1 and CAVIN1 in TMZ-S and TMZ-R cells. Lysates derived from indicated cells were immunoprecipitated by CCBE1 antibody, followed by IB using indicated antibodies. **E.** IP assay of CCBE1 and CAVIN1 interaction in U87 cells treated with or without TMZ for 48 h (left). IB analysis showing CCBE1 in the supernatant (right). **F.** IB detecting CCBE1 expression in cell lysates (left) and supernatant (right) of TMZ-S cell expressing ectopic CAVIN1. **G.** IB assay indicating the expression of CCBE1 in cell lysate (upper) and supernatant (lower) from TMZ-R cells with or without CAVIN1 knockdown. **H.** Tube formation assay of HCMECs treated with CM from U87 cells expressing ectopic CAVIN1 with or without GW4869 treatment ($n = 9$, * $p < 0.05$, ** $p < 0.01$, *** $p < 0.001$). Bars, 100 μ m. **I.** Tube formation assay of HCMECs incubated with CM from TMZ-R cells with CAVIN1 knockdown ($n = 9$, *** $p < 0.001$). Bars, 100 μ m.

phosphorylation (Fig. 5F). Furthermore, the activation of SP1/CCBE1/CAVIN1 regulatory axis and VEGFC/VEGFR/Rho signaling were confirmed in TMZ-R tumors (Fig. 5G) and CCBE1 overexpressed *in vivo* samples treated with or without TMZ (Fig. 5H). Endothelial-to-mesenchymal transition (EndMT) characterized by ECs expressing fibroblast markers is hallmark event for aberrant vasculature formation and chemoresistance in GBM [31–33]. Here, we found that conditioned medium derived from TMZ-R cells with CCBE1 knockdown partially suppressed the EndMT in HCMECs, as represented as the decrease of mesenchymal markers α -SMA/Snail and the retained endothelial marker VE-cadherin (Fig. 5I), and resulted in an inhibition of EMT, as indicated by an increase of *E*-cadherin, and a decrease of

N-cadherin and Vimentin (Fig. 5J). These findings suggested that CCBE1 secretion from GBM cells drives VEGFC/VEGFR/Rho activation and a partial EndMT phenotype in HCMECs. Collectively, the results support a CAVIN1/CCBE1/VEGFC mediated communication between tumor cells and vascular endothelial cells in GBM initiated by chemotherapy that endows TMZ-resistance (Fig. 5K).

4. Discussion

Abnormal neovascularization is a major culprit of cancer progression and treatment resistance [4,33,34]. The current study provides evidence to correlate abnormal neovascularization with TMZ resistance in GBM,

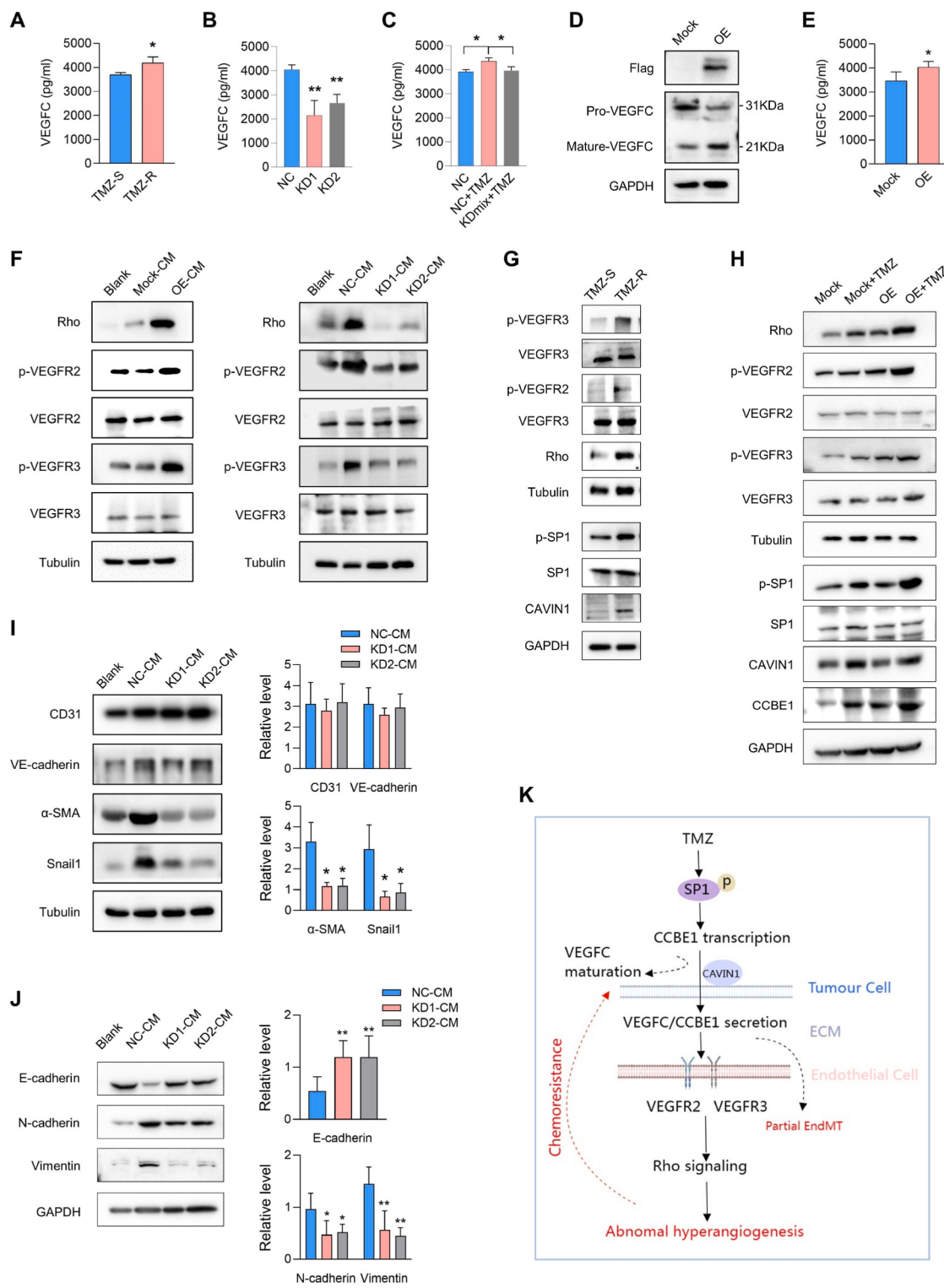


Fig. 5. CCBE1 promotes VEGFC/VEGFR/Rho signaling and EndMT in HCMECs. A. Quantification of VEGFC in the supernatant derived from TMZ-S and TMZ-R cells (n = 3, *p < 0.05). B. Quantification of VEGFC in the supernatant derived from TMZ-R cells with or without CCBE1 knockdown (n = 3, **p < 0.01). C. VEGFC assay of the supernatant derived from U87 cells with or without CCBE1 knockdown (n = 3, *p < 0.05). Cells were treated with TMZ before harvest. D. IB assay of VEGFC maturation in the supernatant of U87 cells expressing Flag-CCBE1 and treated with TMZ using indicated antibodies. E. VEGFC assay of the derived supernatant from cells in D. F. IB assay showing indicated protein expression in HCMECs treated with DMEM or CM from TMZ-S cells with Mock/CCBE1 OE (left) or from TMZ-R cells with or without CCBE1 knockdown (right). G. IB analysis showing the expression of SP1/p-SP1/CAVIN1 expression and VEGFRs/Rho activation in TMZ-S and TMZ-R tumors. GAPDH and Tubulin served as loading controls. H. IB assay detecting the expression of SP1/p-SP1/CAVIN1 and VEGFRs/Rho activation in TMZ-S derived tumors expressing Mock or ectopic CCBE1 treated with or without TMZ. I. IB analysis of EndMT markers in HCMECs treated with indicated CM (n = 3, *p < 0.05, **p < 0.01). J. IB analysis of EMT markers in HCMECs receiving indicated treatment (n = 3, *p < 0.05, **p < 0.01). K. Schematic diagram illustrating the TMZ-induced crosstalk between tumor cells and endothelial cells contributing to hyperangiogenesis and chemoresistance in GBM.

and unveils novel insight into the dynamic interaction between tumor cells and vascular endothelial cells. The regulation axis SP1/CCBE1-/CAVIN1 in tumor cells and CCBE1/VEGFC/VEGFR3/Rho signaling in vascular endothelial cells constructs the cellular and molecular basis of abnormal angiogenesis in chemoresistance in the tumor microenvironment, implying that curbing CCBE1 is key to reversing TMZ resistance.

The constant changes of non-tumor cells from morphology to function constitute a complex TME that accompanies all stages of tumor progression. The adaptive alterations of tumor vascular endothelial cells (TVECs) are not only involved in tumorigenesis and progression, but also contribute to the survival and recurrence of tumor cells upon chemotherapy [34–36]. The current study not only describes the alterations of TVECs and blood vessels in chemo resistant tumors occurs from morphology and number to function, but also discloses that vascular inhibition promotes chemosensitivity. However, due to the holistic suppression of angiogenesis in tumors, Pazopanib used in the present study may not allow for an objective assessment of the contribution of abnormal neovascularization induced by TMZ-therapy to generate and maintain chemoresistance. It's an insurmountable obstacle in this study, however, the restoration of DNA damage capacity to TMZ-R cells indicates that inhibition of chemotherapy-induced abnormal angiogenesis can overcome the development of chemoresistance.

The current finding that CCBE1 upregulation and secretion after TMZ therapy plays a pivotal role in mediating the interaction between GBM cells and TVECs illuminates the cause of abnormal neovascularization due to chemotherapy, consistent with the idea that the interaction between exocytosis factors and their receptors is the main avenue of cellular interactions in TME [37]. CCBE1 functions in extracellular matrix remodeling and is involved in tumor lymphatic metastasis via activation of the VEGFC growth factor signaling pathway, inevitably affecting other cellular alterations, such as remolding the interaction among tumor cells, tumor-associated macrophages (TAMs) [38], and cancer-associated fibroblasts (CAFs) [39,40]. Otherwise, the present study fails to clarify the origin of upstream signaling for SP1 activation-mediated CCBE1 expression. SP1 phosphorylation and constitutive activation may be associated with external signals from senescence-associated secretory phenotype (SASP) induced by chemotherapy [41].

The identified CCBE1 binding protein CAVIN1, also known as polymerase I and transcript release factor (PTRF), interacts with caveolin-1 (CAV1) and regulates caveolae formation, traffic and exosome release [42–44]. Overexpressed CAVIN1 can alter the microenvironment through intercellular communication via exosomes [42]. A recent study reported that disrupting CAVIN1-CAV1 complex inhibits exosome secretion to enhance TMZ efficacy by increasing intracellular concentrations of TMZ [43]. The present observation that CCBE1 excretion was enhanced by TMZ treatment and was affected upon CAVIN1 overexpression or knockdown, suggests disruption of CAVIN1-CCBE1 binding could be a promising therapeutic approach. Furthermore, these backgrounds, as well as the finding that ubiquitination-based degradation of CAVIN1 inhibits the formation of caveolae and exosome secretion [27], provide a possibility that the increase of CCBE1 release is linked to the promotion of stability of CAVIN1 driven by chemo-pressure.

CCBE1 enhances the proteases such as ADAMTS3 (a disintegrin and metalloprotease with thrombospondin motifs-3)-mediated N-terminal cleavage and activation of pro-VEGFC [45]. It contains an EGF domain and a calcium-binding EGF domain (Ca-EGF) at the N-terminus and 2 collagen domains at the C-terminus [46]. The EGF domain of CCBE1 binds ECM, restricting the range of CCBE1 activity and determining the site of VEGFC processing, and the collagen repeat domains activate ADAMTS3, leading to the execution of VEGFC processing. Thus, CCBE1 is involved in VEGFC maturation locally in this way [46]. Additionally, pro-VEGFC binds to VEGFR-3 with the aid of CCBE1 via its EGF domain, and serves as a substrate for ADAMTS3, and subsequently activates VEGFR-3 by mature VEGF-C [45]. Thus, CCBE1 plays a crucial role in proteases mediated VEGFC processing and subsequent VEGFR

activation. Rho GTPases are well addressed to exert important roles in angiogenesis and vascular physiology [47], and the partial EndMT is characteristic cellular behavior for developmental and pathological angiogenesis [48,49]. The current findings corroborate the roles of CCBE1 in VEGFC maturation, VEGFC/VEGFR2/VEGFR3/Rho activation, and EndMT. The regulation on VEGFC/VEGFR/Rho and partial EndMT established an indirect, but close correlation between CCBE1 and pathological angiogenesis in GBM tumors receiving chemotherapy.

Collectively, our findings uncover abnormal neovascularization resulting from the dynamic interaction between vascular endothelial cells directed by a CAVIN1/CCBE1/VEGFC axis. This interaction contributes to chemoresistance and highlights a potential avenue for circumventing the chemoresistance of GBM.

Ethics statement

The study was approved by the Institutional Ethics Committee of The Affiliated Wuxi People's Hospital of Nanjing Medical University.

CRediT authorship contribution statement

Mei Wang: Writing – original draft, Validation, Project administration, Funding acquisition, Formal analysis, Data curation, Conceptualization. **Die Xia:** Methodology, Formal analysis, Data curation. **Daxing Xu:** Resources, Methodology. **Ying Yin:** Supervision, Methodology. **Fei Xu:** Software, Funding acquisition. **Bo Zhang:** Software, Investigation. **Koukou Li:** Visualization. **Zhenkun Yang:** Software, Formal analysis. **Jian Zou:** Writing – review & editing, Visualization, Validation, Supervision, Project administration, Funding acquisition.

Declaration of competing interest

The authors declare that they have no conflicts of interest.

Acknowledgments

This work was supported by Natural Science Foundation of China (NSFC) grants (no. 82172954, 81872056, 81802493, 82003581, 81903391, 82203757 and 82203757), “333” Engineering Project Jiangsu Province ((2022) 2–060), The Natural Science Foundation of Jiangsu Province (Grants No BK20230187, BK20220225), Wuxi Key Medical Talents (ZDRC001), Wuxi Health Committee Youth Program (Grants No Q202135), Wuxi People's Hospital Doctoral Talent Funding (Grants No BSRC202112), General Program of Wuxi Medical Center, Nanjing Medical University (Grants No WMCG202315), Wuxi Science and Technology Development Fund (N20192048), Taihu Talent Plan (JZ), Reserve Talents of Double Hundred Talent Plan (HB2020017, HB2020018), General Program of Jiangsu Commission of Health (M2020012), Wuxi Translational Medicine Research Project (2020ZHJD04). Graphic abstract was developed by Medpeer (<https://image.medpeer.cn/>). We thank Clarity Manuscript Consultants for assistance with language editing (www.claritymanuscripts.com/about.html).

Appendix A. Supplementary data

Supplementary data to this article can be found online at <https://doi.org/10.1016/j.canlet.2023.216593>.

References

- [1] C. Brighi, et al., The potential for remodelling the tumour vasculature in glioblastoma, *Adv. Drug Deliv. Rev.* 136–137 (2018) 49–61.
- [2] A. Bikfalvi, et al., Challenges in glioblastoma research: focus on the tumor microenvironment, *Trends Cancer* 9 (1) (2023) 9–27.
- [3] S.Y. Lee, Temozolomide resistance in glioblastoma multiforme, *Genes Dis* 3 (3) (2016) 198–210.

- [4] H. Kikuchi, et al., Chemotherapy-induced IL8 upregulates MDR1/ABCB1 in tumor blood vessels and results in unfavorable outcome, *Cancer Res.* 80 (14) (2020) 2996–3008.
- [5] Y. Shen, et al., Tumor vasculature remodeling by thalidomide increases delivery and efficacy of cisplatin, *J. Exp. Clin. Cancer Res.* 38 (1) (2019) 427.
- [6] W. Liang, et al., Multiscale modeling reveals angiogenesis-induced drug resistance in brain tumors and predicts a synergistic drug combination targeting EGFR and VEGFR pathways, *BMC Bioinf.* 20 (Suppl 7) (2019) 203.
- [7] M. Bani, et al., Contribution of tumor endothelial cells to drug resistance: anti-angiogenic tyrosine kinase inhibitors act as p-glycoprotein antagonists, *Angiogenesis* 20 (2) (2017) 233–241.
- [8] C. Viallard, B. Larrivee, Tumor angiogenesis and vascular normalization: alternative therapeutic targets, *Angiogenesis* 20 (4) (2017) 409–426.
- [9] G. Eelen, et al., Basic and therapeutic aspects of angiogenesis updated, *Circ. Res.* 127 (2) (2020) 310–329.
- [10] G. Jimenez-Valerio, O. Casanovas, Angiogenesis and metabolism: entwined for therapy resistance, *Trends Cancer* 3 (1) (2017) 10–18.
- [11] S.A. Patel, et al., Molecular mechanisms and future implications of VEGF/VEGFR in cancer therapy, *Clin. Cancer Res.* 29 (1) (2023) 30–39.
- [12] H.J. Cho, et al., VEGF-C mediates RhoGDI2-induced gastric cancer cell metastasis and cisplatin resistance, *Int. J. Cancer* 135 (7) (2014) 1553–1563.
- [13] K.T. Hua, et al., Vascular endothelial growth factor-C modulates proliferation and chemoresistance in acute myeloid leukemic cells through an endothelin-1-dependent induction of cyclooxygenase-2, *Biochim. Biophys. Acta* 1843 (2) (2014) 387–397.
- [14] L. Gong, et al., Characterization of EGFR-reprogrammable temozolomide-resistant cells in a model of glioblastoma, *Cell Death Dis.* 8 (1) (2022) 438.
- [15] M. Wang, et al., Rhox is a novel target for progression and invasion of glioblastoma by impairing cytoskeleton dynamics, *Neurotherapeutics* 17 (4) (2020) 2028–2040.
- [16] J. Jiao, et al., Nuclear Smad 6 promotes gliomagenesis by negatively regulating PIAS3-mediated STAT3 inhibition, *Nat. Commun.* 9 (1) (2018) 2504.
- [17] R. Huang, et al., Identification of key eRNAs for spinal cord injury by integrated multinomial bioinformatics analysis, *Front. Cell Dev. Biol.* 9 (2021), 728242.
- [18] R.W. Robey, et al., Revisiting the role of ABC transporters in multidrug-resistant cancer, *Nat. Rev. Cancer* 18 (7) (2018) 452–464.
- [19] Y. Wang, et al., Extracellular vesicles (EVs) from lung adenocarcinoma cells promote human umbilical vein endothelial cell (HUVEC) angiogenesis through yes kinase-associated protein (YAP) transport, *Int. J. Biol. Sci.* 15 (10) (2019) 2110–2118.
- [20] J.G. Parambil, et al., Pazopanib for severe bleeding and transfusion-dependent anemia in hereditary hemorrhagic telangiectasia, *Angiogenesis* 25 (1) (2022) 87–97.
- [21] Z. Tai, et al., Copper stress impairs angiogenesis and lymphangiogenesis during zebrafish embryogenesis by down-regulating pERK1/2-foxm1-MMP2/9 axis and epigenetically regulating ccbe1 expression, *Angiogenesis* 25 (2) (2022) 241–257.
- [22] S. Parab, R.E. Quick, R.L. Matsuka, Endothelial cell-type-specific molecular requirements for angiogenesis drive fenestrated vessel development in the brain, *Elife* 10 (2021).
- [23] G.A. Tian, et al., CCBE1 promotes GIST development through enhancing angiogenesis and mediating resistance to imatinib, *Sci. Rep.* 6 (2016), 31071.
- [24] S.C. Fletcher, et al., Sp1 phosphorylation by ATM downregulates BER and promotes cell elimination in response to persistent DNA damage, *Nucleic Acids Res.* 46 (4) (2018) 1834–1846.
- [25] S. Iwahori, et al., Identification of phosphorylation sites on transcription factor Sp1 in response to DNA damage and its accumulation at damaged sites, *Cell. Signal.* 20 (10) (2008) 1795–1803.
- [26] N.Y. Tan, L.M. Khachigian, Sp1 phosphorylation and its regulation of gene transcription, *Mol. Cell Biol.* 29 (10) (2009) 2483–2488.
- [27] X. Cen, et al., UBE2O ubiquitinates PTRF/CAVIN1 and inhibits the secretion of exosome-related PTRF/CAVIN1, *Cell Commun. Signal.* 20 (1) (2022) 191.
- [28] G. Wang, et al., A nanounit strategy reverses immune suppression of exosomal PD-L1 and is associated with enhanced ferroptosis, *Nat. Commun.* 12 (1) (2021) 5733.
- [29] G. Wang, et al., Specific fibroblast subpopulations and neuronal structures provide local sources of Vegfc-processing components during zebrafish lymphangiogenesis, *Nat. Commun.* 11 (1) (2020) 2724.
- [30] L. Le Guen, et al., Ccbe1 regulates Vegfc-mediated induction of Vegfr3 signaling during embryonic lymphangiogenesis, *Development* 141 (6) (2014) 1239–1249.
- [31] K.J. Choi, et al., Endothelial-to-mesenchymal transition in anticancer therapy and normal tissue damage, *Exp. Mol. Med.* 52 (5) (2020) 781–792.
- [32] S. Heinzl, [Hormone substitution in menopause], *Med. Monatsschr. Pharm.* 12 (3) (1989) 87–90.
- [33] M. Huang, et al., c-Met-mediated endothelial plasticity drives aberrant vascularization and chemoresistance in glioblastoma, *J. Clin. Invest.* 126 (5) (2016) 1801–1814.
- [34] Z. Wang, et al., The Fibrillin-1/VEGFR2/STAT2 signaling axis promotes chemoresistance via modulating glycolysis and angiogenesis in ovarian cancer organoids and cells, *Cancer Commun.* 42 (3) (2022) 245–265.
- [35] Z. Cao, et al., Angiocrine factors deployed by tumor vascular niche induce B cell lymphoma invasiveness and chemoresistance, *Cancer Cell* 25 (3) (2014) 350–365.
- [36] N. Jhaveri, T.C. Chen, F.M. Hofman, Tumor vasculature and glioma stem cells: contributions to glioma progression, *Cancer Lett.* 380 (2) (2016) 545–551.
- [37] R. Sullivan, et al., The emerging roles of extracellular vesicles as communication vehicles within the tumor microenvironment and beyond, *Front. Endocrinol.* 8 (2017) 194.
- [38] C. Tacconi, et al., Activation of the VEGFC/VEGFR3 pathway induces tumor immune escape in colorectal cancer, *Cancer Res.* 79 (16) (2019) 4196–4210.
- [39] J. Song, et al., The YAP-TEAD4 complex promotes tumor lymphangiogenesis by transcriptionally upregulating CCBE1 in colorectal cancer, *J. Biol. Chem.* 299 (4) (2023), 103012.
- [40] J. Song, et al., CCBE1 promotes tumor lymphangiogenesis and is negatively regulated by TGFbeta signaling in colorectal cancer, *Theranostics* 10 (5) (2020) 2327–2341.
- [41] Y. Hu, et al., The positive regulatory loop of TCF4N/p65 promotes glioblastoma tumourigenesis and chemosensitivity, *Clin. Transl. Med.* 12 (9) (2022) e1042.
- [42] K. Huang, et al., The role of PTRF/Cavin1 as a biomarker in both glioma and serum exosomes, *Theranostics* 8 (6) (2018) 1540–1557.
- [43] B. Hong, et al., EPIC-1042 as a Potent PTRF/Cavin1-Caveolin-1 Interaction Inhibitor to Induce PARP1 Autophagic Degradation and Suppress Temozolomide Efflux for Glioblastoma, *Neuro Oncol.* 2023.
- [44] K.L. Inder, et al., Cavin-1/PTRF alters prostate cancer cell-derived extracellular vesicle content and internalization to attenuate extracellular vesicle-mediated osteoclastogenesis and osteoblast proliferation, *J. Extracell. Vesicles* 3 (2014).
- [45] M. Jeltsch, et al., CCBE1 enhances lymphangiogenesis via A disintegrin and metalloprotease with thrombospondin motifs-3-mediated vascular endothelial growth factor-C activation, *Circulation* 129 (19) (2014) 1962–1971.
- [46] M.G. Roukens, et al., Functional dissection of the CCBE1 protein: a crucial requirement for the collagen repeat domain, *Circ. Res.* 116 (10) (2015) 1660–1669.
- [47] J.N. Kather, J. Kroll, Rho guanine exchange factors in blood vessels: fine-tuners of angiogenesis and vascular function, *Exp. Cell Res.* 319 (9) (2013) 1289–1297.
- [48] J.S. Fang, N.W. Hultgren, C.C.W. Hughes, Regulation of partial and reversible endothelial-to-mesenchymal transition in angiogenesis, *Front. Cell Dev. Biol.* 9 (2021), 702021.
- [49] A.B. Jaykumar, et al., WNK1 collaborates with TGF-beta in endothelial cell junction turnover and angiogenesis, *Proc. Natl. Acad. Sci. U. S. A.* 119 (30) (2022), e2203743119.